Citation for published version:
Ball, RJ, Allen, GC, Starrs, G & McCarter, WJ 2011, 'Impedance spectroscopy measurements to study physio-chemical processes in lime-based composites', *Applied Physics A Materials Science & Processing*, vol. 105, no. 3, pp. 739-751. https://doi.org/10.1007/s00339-011-6509-7

DOI:
10.1007/s00339-011-6509-7

Publication date:
2011

Document Version
Peer reviewed version

Link to publication

The original publication is available at www.springerlink.com

University of Bath

General rights
Copyright and moral rights for the publications made accessible in the public portal are retained by the authors and/or other copyright owners and it is a condition of accessing publications that users recognise and abide by the legal requirements associated with these rights.

Take down policy
If you believe that this document breaches copyright please contact us providing details, and we will remove access to the work immediately and investigate your claim.

Download date: 23. Jan. 2020

Impedance spectroscopy measurements to study physio-chemical processes in lime-based composites

R. J. Ball[ac*] and G. C. Allen[a]

G. Starrs[b] and W. J. McCarter[b]

[a] *University of Bristol, Interface Analysis Centre, 121 St Michael's Hill, Bristol, BS2 8BS*

[b] *Heriot Watt University, School of the Built Environment, Edinburgh, EH14 4AS*

[c] *Currently at: University of Bath, Department of Architecture and Civil Engineering, Bath, BA2 7AY, E-mail: r.j.ball@bath.ac.uk*

**Corresponding author*

Abstract

The conduction and dielectric behaviour of two different grades of natural hydraulic lime is presented over the frequency range 1Hz–1MHz, with measurements taken over the initial 6-months after gauging with water. Samples containing embedded electrodes were exposed to both a natural atmosphere (20ºC and 65% relative humidity) and a natural atmosphere with a carbon dioxide concentration maintained at 400ppm which was used to accelerate the carbonation process. A decrease in relative dielectric permittivity and rise in conductivity, with increasing frequency, was observed at all stages over the time-scale presented. When plotted in the complex plane the impedance featured a bulk response comprising two depressed semicircles and a low frequency spur, the latter being associated with the electrode/sample interface. The complex impedance plot, together with the application of an equivalent circuit model indicated a dual arc feature with carbonation and hydration contributing to bulk impedance response. This study demonstrates the applicability of electrical property measurements to monitor the combined processes of hydration and carbonation in this group of materials.

Keywords: Impedance spectroscopy; lime composites, hydration, carbonation, dielectric permittivity, conductivity.

1. Introduction and Background

This paper describes the application of impedance spectroscopy to study the hardening processes in hydraulic lime composites. Impedance spectroscopy has been applied to a wide range of materials to study their structure and composition. Since its first application to cementitious systems [1] considerable advances have now been made in the use of impedance spectroscopy to study this group of materials [see, for example, 2-11]. Impedance measurements can be interpreted in terms of the mechanisms of hydration, reaction kinetics, microstructural and pore-structure development from initial mixing through setting and long-term hardening. The influence of both chemical admixtures (e.g. accelerators, retarders) and mineral admixtures (e.g. fly ash, ground granulated blast-furnace slag) on the various stages of hydration has also been investigated using impedance spectroscopy techniques. These studies have also shown that the impedance response can be linked to a number of fundamental material properties including pore water content, pore water chemistry, porosity, connectivity and tortousity of the capillary pore network [7].

Surprisingly, little work has been directed towards the application of this testing methodology to hydraulic limes [12]. Whereas cement sets and hardens by chemical reaction with the added water (i.e. hydration), hydraulic lime gains strength by a combination of (slow) hydration and carbonation occurring over a much longer time scale. Pure calcium limes gain rigidity solely through carbonation which can be envisaged as a two stage process – the diffusion of atmospheric carbon dioxide into the lime paste and dissolution within the interstitial water phase to form a weak acid (carbonic acid) followed by the reaction of this acid with calcium hydroxide. These reactions are summarised in equations 1-3 below [13]:

$$Ca(OH)_{2(s)} \rightarrow Ca^{2+} + 2OH^{-} \quad (1)$$

$$CO_2 + H_2O \rightarrow CO_3^{2-} + 2H^{+} \quad (2)$$

$$Ca^{2+} + CO_3^{2-} \rightarrow CaCO_3 \quad (3)$$

As carbonation is a diffusion-based process, reaction kinetics and strength development in lime-based mortars are thus considerably reduced in comparison to a Portland cement-based mortar.

An understanding of the physical and microstructural changes occurring within a lime-based mortar is of considerable importance as these, ultimately, relate to mechanical properties [14-16]. In the current work, samples containing embedded electrodes were manufactured from two grades of natural hydraulic lime (NHL) denoted NHL2 and NHL5. The temporal change in impedance response was measured during exposure to atmospheres with, and without, carbon dioxide. Lime pastes, rather than mortars, were monitored as the absence of the aggregate phase provided better homogeneity and a simpler system for modelling purposes. Electrical property measurements have the considerable advantage of allowing virtually continuous (if required) real-time monitoring on bulk samples at normal temperatures and pressures. Further, the application of impedance spectroscopy to monitor carbonation is timely, due to the current increasing interest of these processes in CO_2 sequestration initiatives. There is also extensive development of techniques to monitor carbonation processes in the fields of cement research and subsurface applications such as nuclear repositories and oil well cements where such materials can be used in backfilling operations.

2. Experimental Method

2.1 Compositional analysis of hydraulic limes

Two hydraulic limes (NHL2 and NHL5 noted above) and a calcium lime, designated CL90, were used and their analysis is given in Table 1. For the purpose of this paper, bulk oxide analysis was carried out by X-ray fluorescence spectroscopy calibrated for the lime oxide proportion. The calcium hydroxide and calcium carbonate content was determined by ignition at 250^{o}C and 950^{o}C respectively, in line with that used in the above procedure.

2.2 Sample manufacture

Two sample geometries were employed in this study, both containing embedded electrodes thereby ensuring intimate contact with the sample. Preliminary studies indicated that samples cast against externally placed electrodes were of limited success due to cracking (hence debonding) at the electrode/sample interface. Two sample types, hereinafter referred to as cuboidal and prismatic, were used in the study and are detailed below.

(a) Cuboidal Samples: this sample type comprised a cube with sides of 40mm. Within each specimen a pair of square electrodes, 20mm×20mm and 1mm thick, were embedded and positioned centrally within the cube. The separation distance between the electrodes within the sample was 20mm. Electrodes were manufactured from Type 316 stainless steel sheet and soldered to 1.6 mm diameter stainless steel wire. The wires were then pushed through tight fitting holes in a 5 mm thick Plexiglas sheet to maintain their orientation and separation while casting within the lime paste. Following casting the samples were placed in the environmental chamber whilst still in their mould. After a period of 7 days the samples were demoulded. The first measurement of impedance was taken after 21 days from the initial mixing. Samples of calcium lime, NHL2 and NHL5 were manufactured as cuboidal samples.

(b) Prismatic Samples: this sample type comprised a lime-paste prism of dimensions 40mm×40mm×60mm (length). For these samples, five faces were coated with a layer of low viscosity epoxy resin thereby sealing the surface and ensuring uniaxial diffusion of carbon dioxide through one of the 40mm×40mm faces. The samples were demoulded after an initial period of 7 days in an environmental chamber containing no carbon dioxide supply and the resin applied. The samples were then left for a further 7 days for the resin to fully harden before being transferred to the environmental chamber with a carbon dioxide supply, this equates to time = 0. Ten pairs of 10mm×10mm×1mm (thick) square, stainless steel electrodes were embedded within each sample. The electrodes within each pair had a separation distance of 10mm. Five electrode pairs were placed in two vertical rows as shown in the schematic in Figure 1. Within each row of electrodes, there was a 'staggered' off-set of 5mm between adjacent pairs; furthermore, there was a 5mm off-set between the two rows. This arrangement of electrode pairs allowed full continuity of impedance measurements from 0-55mm from the exposed end of the prism. A number of prisms without electrodes were manufactured for sectioning and chemical analysis during the experiment. Only NHL2 lime paste was used in the manufacture of prismatic samples.

A water to lime ratio of 1:2 by mass was used throughout as this provided a consistency adequate to provide ease of compaction and embedding of the electrodes without the inclusion of air pockets. The lime and water were mixed in a beaker using a spatula for 10 minutes before casting in steel moulds to form the specimens. Samples were removed from these moulds before impedance measurements were taken. As noted above, a number of

cuboidal samples were manufactured from calcium lime (CL90), however, upon drying it was evident that severe cracking occurred at the electrode/sample interface thereby rendering them unusable in this study.

2.3 Sample exposure

Both types of sample were exposed in Sharetree systems environmental chambers at a temperature of 20^{o}C and relative humidity of 65%. The cubioidal samples were placed in a chamber with no external carbon dioxide supply thereby minimising the rate of carbonation. The prismatic samples were exposed in an environmental chamber with a carbon dioxide supply which was maintained at levels of 400ppm to simulate atmospheric conditions thereby promoting the carbonation reaction.

2.4 Sample monitoring

The impedance response of both sample geometries was monitored at regular intervals over a period of 175 days. Both the in-phase and quadrature components of the sample impedance were determined using a Solartron 1260 impedance analyser, with a signal amplitude of 100 mV over the frequency range 1Hz-1MHz. Impedance values were recorded at 5 frequency measurements per decade. Whilst it was necessary to remove the samples from the environmental chamber during measurement, the duration time out of the chamber was considered negligible so would not affect results. The weight of the cuboidal samples was recorded to an accuracy of 10^{-4}g using a Mettler Toledo AB204-S/FACT digital balance whilst the samples were removed from the environmental chamber for impedance measurements.

The depth of carbonation was determined by sectioning the prism samples without electrodes. The samples were sectioned longitudinally i.e. perpendicular to the face not coated in resin. The depth of carbonation was detected by spraying the freshly exposed surface with a saturated solution of phenolphthalein indicator in ethanol. An estimation of the carbonation depth was then made from the colour change from clear (carbonated) to pink (uncarbonated).

2.5 Environmental scanning electron microscopy

Fracture surfaces of typical microstructures found in the un-carbonated and carbonated regions of the hardened lime pastes were examined using a Philips Electroscan 2020 Environmental Scanning Electron Microscope (ESEM) equipped with a gaseous ion detector. The chamber was evacuated in 'wet' mode (vacuum pressure 5 Torr) and 'flooded' three times to introduce water vapour. Images were then acquired using an accelerating voltage of 20kV. Samples were mounted on 12 mm diameter pin-stubs coated with silver dag. Fracture surfaces of regions from each sample were then sputtered with gold using an Edwards sputter coater for a period of 4 minutes thereby enhancing contrast.

3. Impedance analysis

3.1 Finite element analysis of current flow

To provide a basis for determining the conductivity and relative dielectric permittivity (or dielectric constant) of the samples, it was necessary to determine the current flow and potential distribution within the sample. As a result of the complex electrode geometry, a closed form solution was not readily available so a finite element analysis was used employing AnSys simulation software (ANSYS, Inc. Southpointe 275 Technology Drive, Canonsburg, PA 15317, Software Version No 11). Ansys solves three dimensional problems by applying Laplace's equation [17], which can be used for solving a wide range of continuous physical processes including the distribution of electric potential within a medium. For more detailed information on the solution techniques the reader is referred to the AnSys guides (ANSYS Theory Reference, Chapter 6, 000855. 8th Edition, SAS IP, Inc©). The element type used for the electrical analysis, was a three-dimensional solid 'brick' element, referred to in the AnSys guide as *SOLID70*. Following generation of the solution, post processing in AnSys allows calculation of the magnitude of the resultant flux which can be represented in the form of vectors or contour plots. The vector and contour plots obtained from the cube sample geometry are shown in Figure 2 and show the field fringing effects around the embedded electrode system. In the current analysis, properties of the lime paste were assumed to be isotropic i.e. the effect of localized and temporal changes in current distribution are not considered in this current model. The results obtained from the model

were used to calculate a geometrical conversion factor, F, which allowed calculation of conductivity and dielectric permittivity by taking account of current flow outside of the volume of material directly between the electrodes being monitored. In the absence of this factor the calculated values of conductivity and dielectric permittivity would be overestimated. Values of 0.31 were obtained for the cuboidal sample. For the prismatic sample a value of 0.3 was used for the electrode pairs at the end positions, 0 and 45 mm, 0.25 for the electrode pairs at the 5 and 40 mm positions and 0.22 for electrode pairs positioned between 10-35 mm from the exposed surface. The constant, k, used in equations 5 and 6 below is then calculated using $k = Fd/A$, where d is the electrode spacing and A is electrode area.

3.2 Equivalent circuit modelling

The electrical response of the lime pastes was simulated using an equivalent circuit model in ZView software version 2.90 (Scribner Associates, Inc.). The circuit used is presented in Figure 3 and consists of resistors (R) and constant phase elements (CPE). The constant phase element (CPE) does not have an electrical equivalent and is a complex, frequency-dependent parameter defined by the relationship, equation (4),

$$CPE = A_o(i\omega)^{-n} \qquad (4)$$

where $i = \sqrt{-1}$, A_o is a constant and the exponent, n, has a value such that $0<n<1$; if n equals 1 then the equation is identical to that of a pure capacitor of value A_o. When a CPE, with value of $n<1$, is placed in parallel with a resistor, a Cole-Element (depressed semi-circle) is produced in the complex plane. The use of a CPE in place of a capacitor thus accounts for dielectric dispersion in the system.

3.3 Calculation of electrical parameters

Connection to the Solartron impedance analyser was by means of short, individually screened coaxial cables to the voltage High/Low and current Output/Input terminals. Open circuit and short circuit measurements were taken at all test frequencies; from this set of measurements, together with the impedance of the sample between the electrodes, the sample impedance can

be de-embedded from the measured impedance. However, it was found that open circuit impedances were significantly higher, and short circuit impedances significantly lower, than those recorded for the specimens indicating that the contribution of the residual cable impedance would be negligible. The sample impedance, Z(ω) at any frequency, ω, can be written as,

$$Z(\omega) = Z'(\omega) - iZ''(\omega) \tag{5}$$

where the values of $Z'(\omega)$ and $Z''(\omega)$ are the in-phase and quadrature components of the measured impedance.

The relative dielectric permittivity (ε'_r) and conductivity (σ) of the sample at any frequency, ω, are calculated using equations (6) and (7) below. In these equations, k is the factor to account for fringing effects for the particular electrode configuration (obtained from Ansys) and ε_o is the permittivity of a vacuum (8.854×10^{-12} Farads/m).

$$\sigma(\omega) = \frac{Z'(\omega)}{\left(Z'(\omega)^2 + Z''(\omega)^2\right)} \cdot k \tag{6}$$

$$\varepsilon'_r(\omega) = \frac{Z''(\omega)}{\varepsilon_o \omega \left(Z'(\omega)^2 + Z''(\omega)^2\right)} \cdot k \tag{7}$$

4. Results

4.1 Material composition

The oxide equivalent and derived phase composition of the NHL2 and NHL5 limes is given in Table 1. An analysis of the CL90 calcium lime is also included for completeness however, as stated earlier, cracking at the specimen/electrode interface rendered these specimens unusable. The NHL5 contains approximately three times more dicalcium silicate (C_2S) compared to the NHL2 which accounts for its greater hydrolicity. Approximately 2.5 times more portlandite is present in the NHL2 compared to NHL5 giving it a much greater potential to carbonate. Interestingly, a greater quantity of calcium alumino-silicate (C_2AS) was

detected in the NHL2. Approximately 20% calcite was present in both limes with the other phases in much lower amounts.

4.2 Microstructure, carbonation and weight change

Microstructures relating to the NHL2 and NHL5 lime pastes at 175 days in the uncarbonated and carbonated states are given in Figure 4 (a)-(d). It should be noted that, in this context, carbonated and uncarbonated relate to pastes which when sprayed with phenolphthalein indicator are clear (pH < 10) and pink (pH > 10) respectively. Uncarbonated lime paste was taken from the central region of the specimen and carbonated lime paste from approximately 3 mm below the outer surface of the specimen. Figures 4 (a) and (b) show typical carbonated and uncarbonated structures of the hardened NHL2 lime pastes. There are no obvious differences between the two images as both contain agglomerated lime particles and high aspect ratio needle shaped crystals. Figures 4(c) and (d) correspond to the uncarbonated and carbonated structures observed for the NHL5 lime paste. High aspect ratio crystals are, again, observed in both images however these are approximately 1μm in length making them significantly smaller than those observed in the NHL2. A number of well defined angular crystals are distributed throughout the carbonated sample. Some of these take the form of hexagonal Portlandite plates and are the by-product of C_2S hydration as shown in equation (8) below,

$$2Ca_2SiO_4 + 4H_2O \rightarrow Ca_3Si_2O_7.3H_2O + Ca(OH)_2 \qquad (8)$$

The mass of the cuboidal specimens was recorded throughout the exposure period at the same time impedance measurements were taken. The average mass of the calcium lime, CL90, specimens at 21 and 175 days was 59.7g and 68.0g respectively; the NHL2 and NHL5 hydraulic limes at 21 days were, respectively, 79.0g and 97.9g, and at 175 days, 82.4g and 97.6g. The percentage change in weight throughout the monitoring period relative to the weight at 21 days is presented in Figure 5. The greatest increase in weight was observed in the CL90 followed by the natural hydraulic lime, NHL2. A small decrease in weight was measured for the natural hydraulic lime NHL5. The maximum percentage change in weight recorded for the natural hydraulic lime mortars was 4.3 % for the NHL2. The weight

increases are likely to be due to carbonation and also indicates that no significant evaporation of water from the samples has occurred during the monitoring period.

4.3 Conductivity and Dielectric Permittivity

As noted above, the intrinsic electrical properties of any non-magnetic material can be fully specified by the frequency dependent parameters, relative dielectric permittivity, $\varepsilon_r'(\omega)$, and conductivity, $\sigma(\omega)$. These are determined by the polarization and conduction of bound and free charges within the material. If the material is heterogeneous, $\varepsilon_r'(\omega)$ and $\sigma(\omega)$ will be strongly correlated to the properties of the individual components and the way in which they are combined. Such correlation is often manifested in the frequency domain as dispersive behaviour characterised by frequencies of relaxation, above which dielectric permittivity falls and conductivity rises. It can therefore be possible to identify various features of heterogeneous materials by their electrical properties provided these are observed over a wide enough frequency range

The dielectric permittivity and conductivity are presented in Figure 6 for NHL2 and NHL5 pastes, and plotted in the frequency domain. This plot represents a typical response from the cuboidal samples. Figure 7 presents the corresponding response from the NHL2 prismatic samples for electrode pairs positioned respectively at 5mm and 35mm from the exposed surface. All plots display a decrease in dielectric permittivity and rise in conductivity with increasing frequency.

The dielectric permittivity gives a relative measure of the electric polarizability of the system and, at any particular frequency of applied field, quantifies the sum of all polarization processes operative within the material. Several superimposed mechanisms can contribute to polarization with each one having a characteristic relaxation frequency. In the lime pastes, it is evident from Figure 6 that dispersion in the dielectric permittivity exists across the entire frequency range under study and is indicative of a spread of relaxation frequencies. With reference to Figure 6, at low frequencies (<10Hz) the dielectric permittivity rises to anomalously high values: ~10^5 for NHL2 pastes (Figure 6(a)) and ~10^6 for NHL5 pastes (Figure 6(b)), but can be explained by the dominating influence of electrode polarization below this frequency. Also noticeable for both types of lime pastes is the development of a

small 'plateau' region over the frequency range ~1kHz-50kHz which becomes more discernible with increasing hardening time. The dielectric permittivity then undergoes a further dispersion over the range ~50kHz-1MHz (1MHz being the upper limit of the current investigation). Concerning the bulk polarization processes operative within the paste, it is proposed that this results from a combination of electric double-layer polarization and an interfacial polarization processes occurring within the paste. Both these mechanisms relax in the frequency range of the current investigation; however, since double-layer polarization is a low-frequency mechanism [18] and interfacial polarization a mid-frequency mechanism [19] it could be postulated that the plateau region delineates these processes. The double-layer process and electrode polarization effects will merge together at the low-frequency end of the Figure hence it is difficult to accurately identify the frequency above which double-layer effects start to dominate.

Regarding the above polarization mechanisms, double layer polarization on particle surfaces has been known to produce substantial dielectric enhancement at low frequencies for colloidal suspensions [18, 20, 21] and porous materials saturated with conductive liquids [22], the latter using a grain consolidation model. Interfacial polarization would manifest itself at the pore-water/crystal boundary interfaces. Under the application of an electric field, charges can be *blocked* by internal phase boundaries leading to a separation of charge which will contribute to the polarizability of the sample. With the system under study, the paste can be considered as a two-phase system comprising solid phase (e.g. products of hydration, unreacted materials) and an interstitial aqueous phase; as these phases will be electrically dissimilar this would give rise to a Maxwell-Wagner interfacial polarization process. As the lime pastes increase in rigidity due to hydration (equation (8) above) the pore network will become more tortuous and constricted with the carbonation process (equations (1)-(3) above) also serving to block pore connectivity [23]; free water taken up in the chemical reactions will also result in an irrotational binding of water. These physio-chemical processes will cause an overall reduction in bulk polarisation, hence dielectric permittivity, across the entire frequency range.

Conductivity quantifies the sum of all loss mechanisms operative within the system and represents the energy dissipated by the motion of charges in the applied field. For the lime pastes these losses would include the movement of free charges in the continuous, interstitial

aqueous phase which results from ionic conduction. However, losses associated with polarization processes operative within the paste will also contribute to the measured conductivity. Where dielectric relaxation processes are operative this would result in an enhancement of conductivity with increasing frequency. With reference to Figure 6, the conductivity decreases with time and increases with frequency across the entire frequency range; its response can be divided into three regions:

(i) a region between 1-10Hz where the conductivity increases with increasing frequency (more evident in Figure 6(b) for the NHL5 paste). In this region the conductivity will be influenced by processes at the electrode-sample interface.
(ii) a region between ~10Hz-50kHz, where the conductivity gradually increases in a linear fashion; and,
(iii) a region >50kHz where the dispersion in conductivity increases more markedly, again in a linear fashion.

Within the frequency range ~10Hz-1MHz, it is proposed that conduction will be dominated by ionic conduction through the continuous interstitial aqueous phase. Superimposed on this mechanism will be contributions from double-layer relaxation over the range 100Hz-50kHz, albeit a very weak contribution, and strong contribution from interfacial polarization at frequencies >50kHz. As with the dielectric permittivity, the overall reduction of conductivity with time can be attributed to the increase in rigidity of the paste resulting from the hydration and carbonation processes discussed above. .

Figures 6(a) and (b) also indicate that the conductivity and dielectric permittivity of NHL5 lime paste is almost an order of magnitude higher than that of the NHL2. This will be as a result of compositional differences between the two materials (see Table 1) and consequent higher ionic content in the interstitial water phase within NHL5 paste, through which conduction occurs. Comparing Figure 6(a) and (b) it is evident that there is a more marked decrease in dielectric constant and conductivity over the period 21-35 days for the NHL5 paste. The NHL5 paste has a higher proportion of C_2S phase which contributes to the hardening process; although slow to hydrate initially, it is evident from the dielectric permittivity and conductivity response presented in Figure 6(b) that this reaction (equation (8)) begins to take effect over this time.

Figs. 7(a) and (b) present the dielectric permittivity and conductivity at the electrode pairs positioned at depths of 5mm and 35mm in the NHL2 prismatic samples. Considering the dielectric permittivity response, it is evident that these Figures provide more detail on the regions of dispersion than their cuboidal counterparts presented in Figure 6. Whereas the cuboidal samples will represent an overall 'bulk' response, the smaller volume of material probed by the electrodes in the prismatic sample will be more sensitive to physio-chemical changes occurring within the paste. With reference to Figure 7, the dielectric dispersion curves change slope at $\sim 10^2$Hz, then again at $\sim 10^4$Hz, thereafter the dielectric permittivity decreases over the remainder of the frequency range. It could be postulated that these frequencies delineate three polarization processes: electrode polarization dominating at frequencies < $\sim 10^2$Hz; double-layer polarization dominating over the range $\sim 10^2$ - 10^4Hz, and interfacial polarization dominating at frequencies > $\sim 10^4$Hz which is also the frequency at which dispersion in conductivity is more evident.

From Figure 7, the conductivity and dielectric permittivity at a depth of 5mm are reduced in comparison to the values at 35mm. This is attributed to carbonation resulting from the diffusion of CO_2 into the surface zone

4.4 Equivalent circuit modelling

The complex impedance formalism for data presentation is useful in developing an equivalent circuit representation for the system. Figure 8(a) shows a typical response for the prismatic NHL2 paste after 12 days. Figures 8(b) and (c) show typical responses for the NHL2 and NHL5 pastes from the cuboidal samples. In these figures frequency is increasing from right to left across the arcs.

Considering Figure 8, the spectra for hydraulic lime pastes can be separated into two overlapping arcs whose centres are displaced below the real axis: a mid-frequency arc developing over the frequency range ≈100Hz-100kHz and a high-frequency arc developing over the frequency range 100kHz-1MHz. These arcs represent the material response, with a small 'spur' at the right-hand-side of the plot representing the low-frequency response at the electrode-sample interface. As noted above, an equivalent circuit of the form shown in Figure 3 was applied to the data for simulation purposes. Researchers have used similar

equivalent circuits to represent cementitious and other ceramic materials [2-8, 18, 24-26] as it allows deconvolution of the resistance, R, and constant phase element parameters, A_o and n in equation (4) above, from both the left- and right- hand side of the bulk response, namely R1/CPE1 (high frequency) and R2/CPE2 (mid-frequency) on Figure 3, with R3/CPE3 representing the electrode response. Table 2 presents the modelled circuit parameters for the bulk response presented in Figures 8(a)-(c); values for R3/CPE3 are not reported. Figure 9 displays the temporal changes in R1 and R2 for the NHL2 and NHL5 cuboidal samples over the period 21 to and 175 days. These resistances will be associated with, (a) the continuous capillary pathways between the electrodes i.e. the percolating pores or connected porosity; and, (b) those capillary pores which do not connect between the electrodes i.e. the dead end pores and occluded porosity [27]. Thus, as the capillary pores become more tortuous and disconnected due to hydration and carbonation processes, these values will increase with time as shown in Figure 9. Further work (in combination with MIP studies) is required, however, to ascribe the contribution of a particular pore type (e.g. continuous, occluded) and the distribution of pore types to the resistance parameters R1 and R2.

When plotted in the complex impedance plane, the dispersive and relaxation processes discussed in relation to Figures 6 and 7 appear to manifest themselves as a two region response comprising an electrode polarisation 'spur' on the extreme right of the plot (at frequencies < ≈100Hz) and a bulk response on the left of the cusp point. The bulk response, itself, displays a *dual*-arc behaviour. At the permittivity level (see Figure 7(b)) the weakly defined plateau centered around ~10kHz is followed by a second dispersion up to 1 MHz which was the limit of the current investigation. This indicates the possible existence of two relaxation processes in addition to the diffusion limited polarization process associated with the electrodes. *The* primary region of dispersion (frequencies > ~100Hz) which has resulted in two bulk arcs is viewed at the impedance level in Figure 8.

4.5 Movement of the Carbonation Front

Figure 10 presents a contour plot of the bulk resistivity (based on R1+R2 values) for all electrode pairs located in the NHL2 prismatic samples. Over the time-scale presented, two features are discernible,

(i) an overall uniform increase in resistivity with time at all electrode positions; and

(ii) a more significant increase for electrodes positioned at 0 and 5mm from the surface which becomes more prominent after 61 days.

Insets on the right of the contour plot show stained sections of the prismatic sample indicating the depth of carbonation at 39 and 161 days. An intense purple staining is observed at 39 days across the whole of the sample with only a thin 2mm carbonated zone present on the left hand side corresponding to the unsealed face. In comparison, white speckles are visible on the surface of the 161 day old section indicating greater carbonation throughout the entire volume. The carbonated region has grown to approximately 12 mm in thickness which coincides with electrodes in the 0 and 5 mm positions where high resistance was measured. This increase in resistance is not attributable to loss of moisture from the samples as their weight remains relatively constant over this period (see Figure 5). The deeper electrode positions will reflect the hydraulic hardening effect of the pastes, whereas the surface electrodes (i.e. at 0 and 5mm) will reflect a combined hardening effect of the lime hydraulicity and carbonation.

6. Concluding Comments

The change in the electrical properties of natural hydraulic lime pastes have been presented over a period of six months from initial gauging. Measurements have been presented in a range of formalisms to highlight the frequency dependence of the electrical response for this group of materials which included complex impedance, dielectric permittivity and conductivity. Regarding the complex impedance, in the Argand plot, the bulk response gave rise to two arcs together with a low-frequency arc associated with electrode polarization effects. The bulk arcs had their centres depressed below the real axis which is indicative of frequency-dependent behaviour of the capacitive element i.e. a constant phase element varying as $A_o(i\omega)^{-n}$.

When plotted as the dielectric permittivity there was, what appeared to be, a single region of dispersion across the entire frequency range under study with a small plateau region evident in the range 1kHz-50kHz. It was postulated that region delineated two processes: a low-frequency double-layer polarization process and a higher frequency interfacial mechanism. At this stage, it was difficult to evaluate the exact relaxation frequency for each process due to the upper frequency limit of the investigation and, at the low-frequency end of the

investigation, the increasing influence of electrode effects masking the bulk polarization process. The conductivity, which quantifies the sum of all the loss-processes, displayed a three-region response associated with electrode effects, ionic conduction and losses due to dispersive polarization processes.

Considering the prismatic sample exposed to carbon dioxide, it was evident that the surface electrodes indicated a region of high resistivity resulting from a combination of carbonation and hydraulic hardening of the lime.

7. Acknowledgements

Thanks are due to Chris Bowen at the University of Bath for use of Ansys finite element modelling software and Hanson Cement. (Clitheroe, Lancashire, UK) for supply and analysis of materials. The support of the Engineering and Physical Sciences Research Council, UK, is gratefully acknowledged.

8. References

[1] McCarter W J, Garvin S and Bouzid N, 1988, *J. Mat. Sci. Lett*. **7** 1056-7

[2] Andrade C, Blanco V M, Collazo A, Keddam M, Novoa X R, Takenouti H, 1999, *Electrochimica Acta* **44** 4313-4318

[3] McCarter W J and Brousseau R, 1990, *Cem. Concr. Res.* **20** (6) 891-900

[4] McCarter W J, Chrisp T M and Starrs G, 1999, *Cem. Concr. Comp*. **21** 277-83

[5] McCarter W J, Starrs G and Chrisp T M., 2002, *Electrical monitoring methods in cement science. In Structure and Performance of Cements', J. Bensted and P. Barnes (Eds)* (SPON) 442-56 ISBN 0 419 23330 X

[6] Scuderi C A, Mason T O and Jennings H M, 1991, *J. Mat. Sci.* **26** 349-353

[7] Xie P, Gu P, Xu Z and Beaudoin J J, 1993, *Cem. Conc. Res.* **23** 359-67

[8] Christensen B J, Coverdale R T, Olson R A, Ford S.J, Garboczi E J, Jennings H M and Mason T, 1994, *J. Am. Ceram. Soc*. **77** 2789-804

[9] Macphee, D.E., Sinclair, D.C. and Stubbs, S.L., 1996, J. Mat. Sci. Lett, 15 (18), 1566-8

[10] Macphee, D.E., Sinclair, D.C. and Stubbs, S.L., 1997, J. Am. Ceram. Soc., 80 (11), 2876-84

[11] Cormack, S. L., Macphee, D. E. and Sinclair, D. C., 1998, Adv. in Cement Research, 10 (4), Oct, 151-160

[12] Allen G C, Allen J, Elton N, Farey M, Holmes S, Livesey P and Radonjic M, 2003, *Hydraulic Lime Mortar for Stone, Brick and Block Masonry* (Donhead) ISBN 1-873394-64-0

[13] Montes-Hernandez G., et al. Journal of Crystal Growth (2008) 310, 2946-2953.

[14] Ball R J, El-Turki A, Allen, W J and Allen, G C, 2007 *Const. Mat. Proc. Instn. Civil Eng*. **CM2,** 57-63

[15] Ball R J and Allen G C,*2009, Int. J. of Sust. Eng*. iFirst article 1-7 DOI:10.1080/19397030903191219

[16] El-Turki A, Carter M A, Wilson M A, Ball R J, and Allen G C, 2009, *Const. and Build. Mat.* **23** 1423-1428

[17] Zienkiewicz O C ,1971, *The Finite Element Method in Engineering Science* (McGraw Hill) ISBN 0070941386

[18] Schwan P, Schwarz G, Maczuk J and Pauly H, 1962, *J. Physical Chem*. **66** 2626-35

[19] Hasted J. B., 'Aqueous Dielectrics', Chapman and Hall, London, 1973, 286

[20] Schwarz G, 1962 *J. Physical Chem*. **66** 2636-42.

[21] Chew W C and Sen P N 1982 *J. Chemical Phy.* **77** (9) 4683-93

[22] Nettelblad B. and Niklasson G. A., 1997 *J. of Matls. Sci*. **32** 3783-3800

[23] Daval D, Martinez I, Guigner J-M, Hellmann R, Corvisier J, Findling N, Dominici C, Goffé B and Guyot F, 2009, American Mineralogist **94** 1707-1726.

[24] Kim S and Hwang J-H 2006 *J. Korean Ceram. Soc*. **43** (3) 156-61

[25] Edwards, D. D., Hwang, J-H, Ford, S. J. and Mason, T. O., 1997 *Solid State Ionics* **99** (1-2) 85-93

[26] Ford S J, Hwang J-H, Shane J D, Olson R A, Moss G M, Jennings H M, and Mason T O, 1997, *Adv. Cem. Based Mat*. **5** (2) 41-48

[27] McCarter W J and Garvin S, 1989, *J. Phys. D: Appl. Phys.* **22** 1773-1776.

Captions for Figures

Figure 1: Electrode array embedded into NHL2 hydraulic lime prismatic sample. (a) schematic diagram showing positioning of electrode pairs; and (b) photograph of array.

Figure 2: Solution of finite element model for 40×40×40mm cube containing 20×20mm electrodes embedded 20mm apart centrally (a) vector plot showing magnitude and direction of current flow and (b) contour plot (from section between electrodes) showing variation in current density.

Figure 3: Equivalent circuit model with R1/CPE1 and R2/CPE2 representing the bulk response and R3/CPE3 representing the electrode response.

Figure 4: Environmental scanning electron micrographs illustrating typical fracture surfaces of the uncarbonated and carbonated regions of NHL2 and NHL5 lime pastes (at 175 days); (a) NHL 2 uncarbonated; (b) NHL2 carbonated; (c) NHL5 uncarbonated; and (d) NHL5 carbonated (scale bar represents 4μm).

Figure 5: Relative change in weight for calcium lime and natural hydraulic lime, NHL2 and NHL5, cuboidal samples during the monitoring period (21 day weight taken as datum).

Figure 6: Typical plots of dielectric permittivity and conductivity for cuboidal samples of (a) NHL2, and (b) NHL5, between 21 and 175 days.

Figure 7: Typical plots of dielectric permittivity and conductivity for electrode pairs in a prismatic sample, (a) 5 mm location, and (b) 35 mm location, between 0 and 161 days.

Figure 8: Typical complex plane plot and equivalent circuit parameters from simulation (a) prismatic NHL2 paste (at 5mm) after 12 days; (b) cuboidal NHL2 paste after 147 days and (c) cuboidal NHL5 paste after 147 days

Figure 9: Values of R1 and R2 obtained from equivalent circuit modelling of complex plane plots obtained from (a) NHL2 and (b) NHL5 cuboidal samples.

Figure 10: Contour plot showing resistivity of NHL2 lime paste between electrode pairs embedded in the prismatic samples. Images to the right show depth of carbonation revealed by phenolphthalein indicator.

Captions for Tables

Table 1. Chemical composition of calcium lime CL90 and natural hydraulic limes, NHL2 and NHL5.

Table 2. Modelled circuit parameters for the bulk response presented in Figures 8(a)-(c); values for R3/CPE3 are not reported.

Table 1. Chemical composition of calcium lime CL90 and natural hydraulic limes, NHL2 and NHL5.

Chemical composition (% w/w)	**CL90**	**NHL2**	**NHL5**
SiO_2	0.8	11.4	19.9
Al_2O_3	0.1	1.7	2.0
Fe_2O_3	0.1	0.5	0.7
CaO	73.6	61.2	59.8
MgO	0.9	2.4	1.2
K_2O	0.02	0.39	0.42
Na_2O	0.0	0.06	0.03
SO_3	0.0	1.16	0.36
Cl	0.0	0.01	0.01
Loss on ignition	24.4	21.2	15.4
Total	*100*	*100*	*99.78*
Insoluble residue	0.9	2.7	3.7
Calcination loss	-	8.4	10.2
Soluble SO_3	-	0.32	<0.01
Relative density	2.24	2.4	2.69
Soluble SiO_2	-	5	12.5
C_2S	0.0	14.3	45.0
$Ca(OH)_2$	97.1	53.6	20.6
$CaCO_3$	0.0	21.7	23.1
$CaSO_4$	0.0	1.5	0.0
C_4AF	0.0	1.7	2.0
C_3A	0.0	0.7	2.1
C_2AS	0.0	3.4	2.2
Total	*97.1*	*99.6*	*98.7*
Cementation index	-	0.3	0.78

Table 2. Modelled circuit parameters for the bulk response presented in Figures 8(a)-(c); values for R3/CPE3 are not reported.

Sample	Time (days)	R1 (high) kΩ	R2 (mid) kΩ	CPE1 (high)		CPE2 (mid)	
				A_o ($\times 10^{-10}$)	n	A_o ($\times 10^{-9}$)	n
NHL2 (prismatic at 5mm)	12	42.2	55.7	0.549	0.83	7.71	0.66
NHL2 (cuboidal)	147	36.3	19.2	5.41	0.71	1.20	0.87
NHL5 (cuboidal)	147	17.7	19.7	36.0	0.63	0.72	0.92

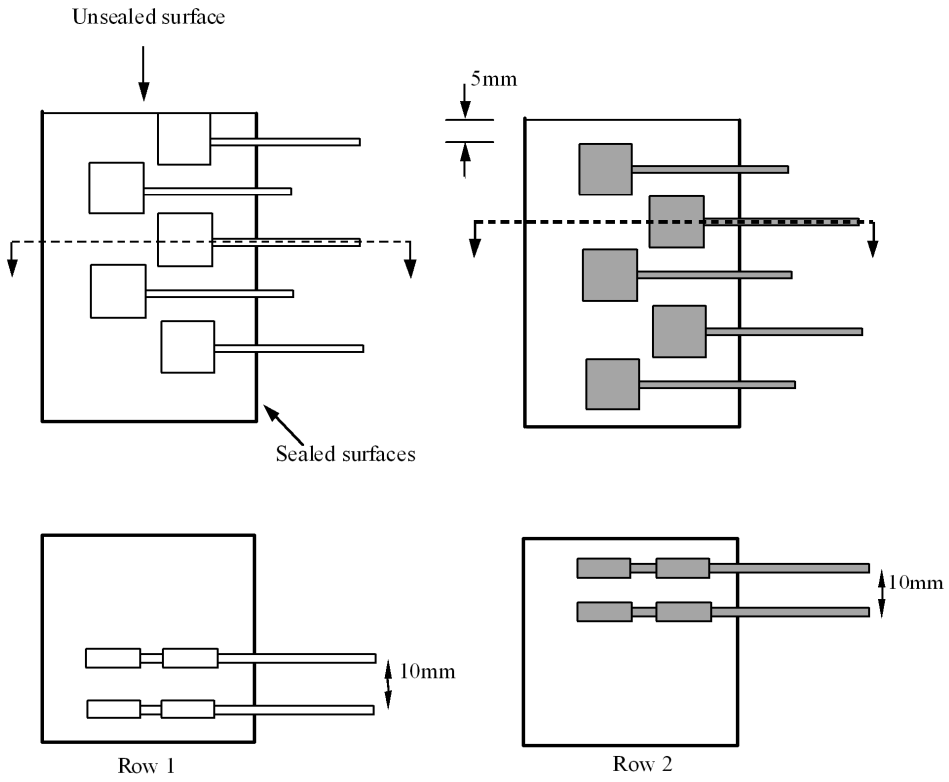

(a)

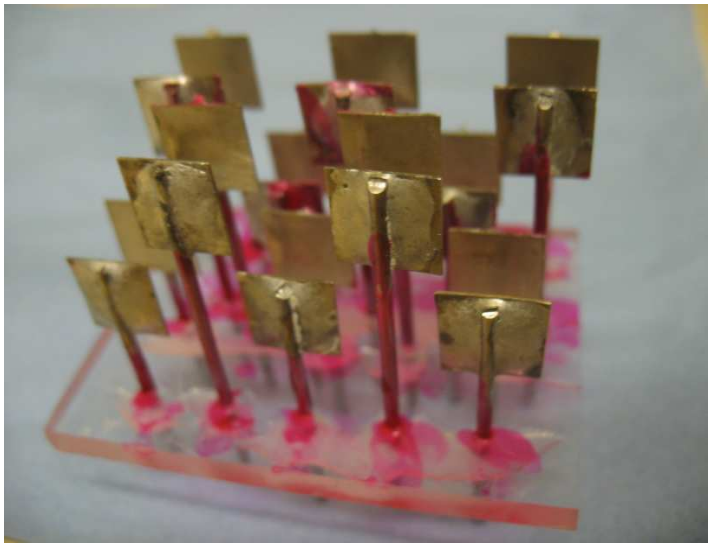

(b)

Figure 1: Electrode array embedded into NHL2 hydraulic lime prismatic sample. (a) schematic diagram showing positioning of electrode pairs; and (b) photograph of array.

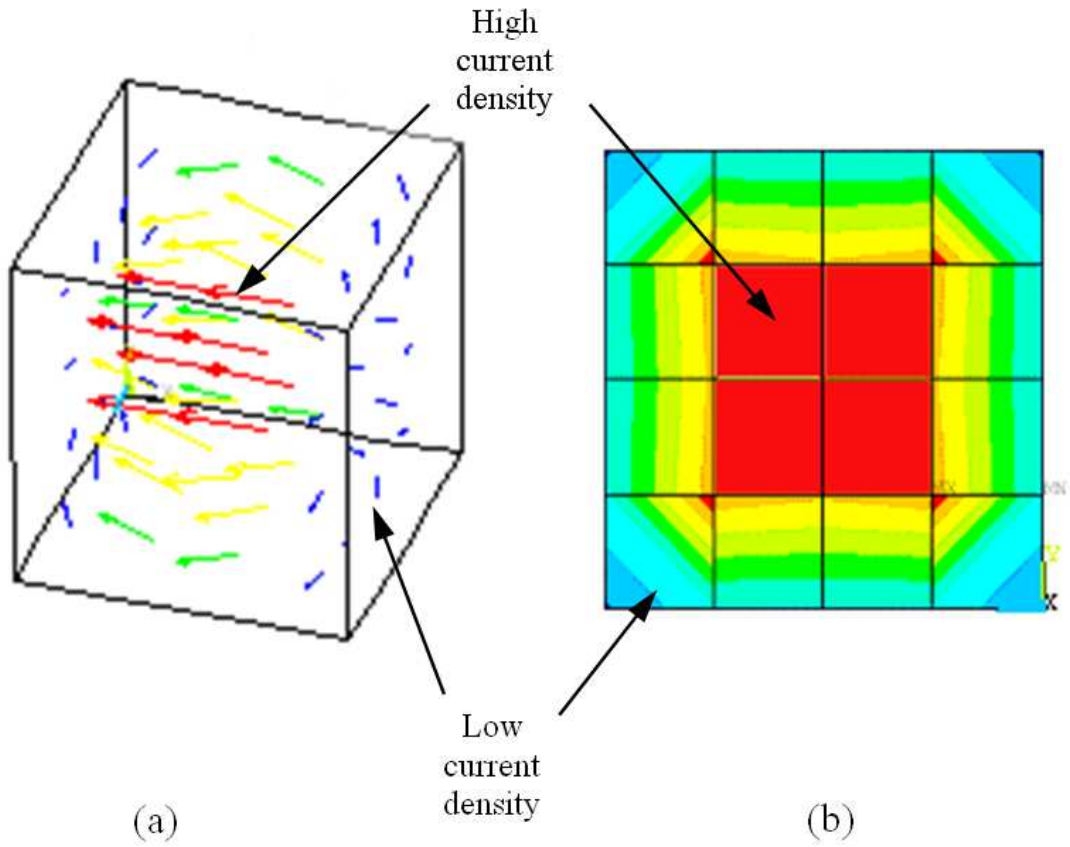

Figure 2: Solution of finite element model for 40×40×40mm cube containing 20×20mm electrodes embedded 20mm apart centrally (a) vector plot showing magnitude and direction of current flow and (b) contour plot (from section between electrodes) showing variation in current density.

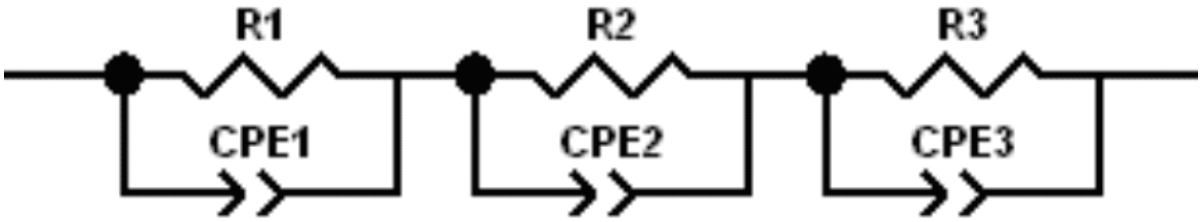

Figure 3: Equivalent circuit model with R1/CPE1 and R2/CPE2 representing the bulk response and R3/CPE3 representing the electrode response.

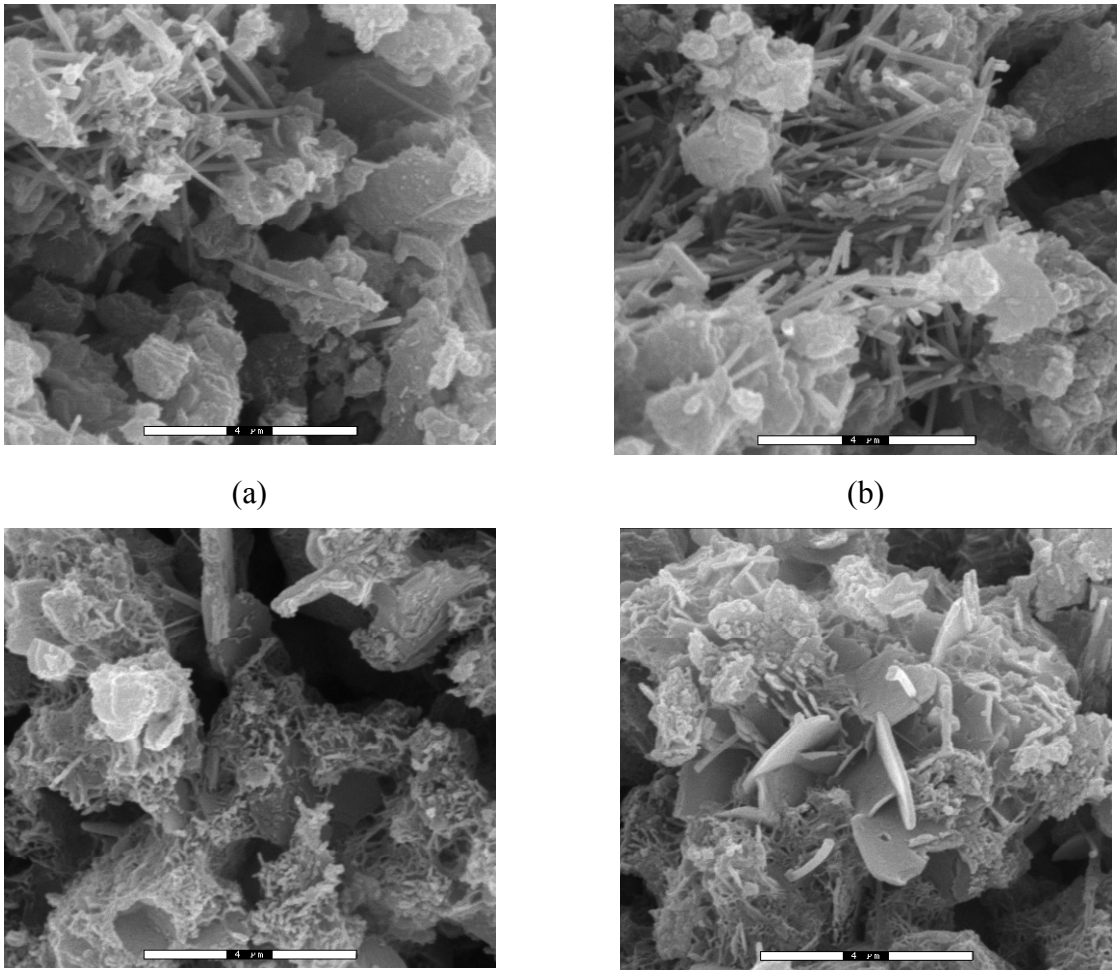

(a) (b)

(c) (d)

Figure 4: Environmental scanning electron micrographs illustrating typical fracture surfaces of the uncarbonated and carbonated regions of NHL2 and NHL5 lime pastes (at 175 days); (a) NHL 2 uncarbonated; (b) NHL2 carbonated; (c) NHL5 uncarbonated; and (d) NHL5 carbonated (scale bar represents 4μm).

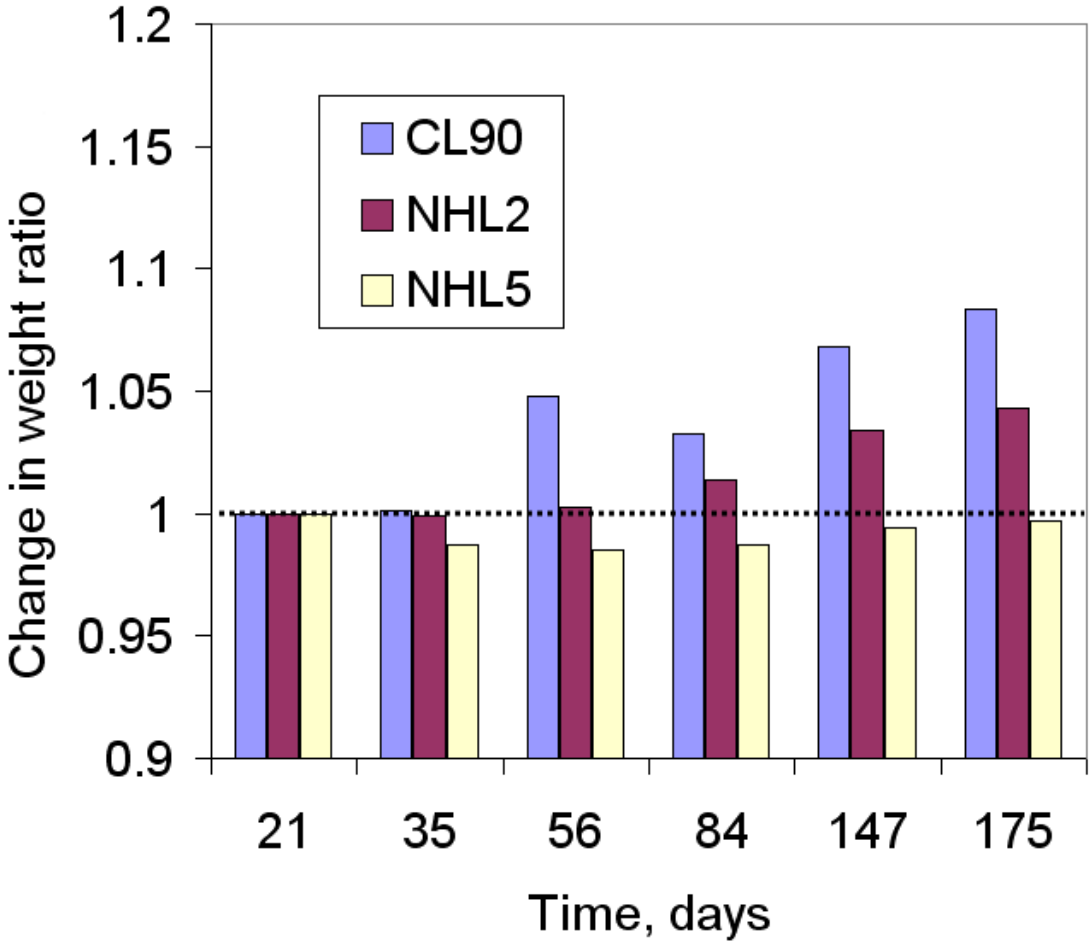

Figure 5: Relative change in weight for calcium lime and natural hydraulic lime, NHL2 and NHL5, cuboidal samples during the monitoring period (21 day weight taken as datum).

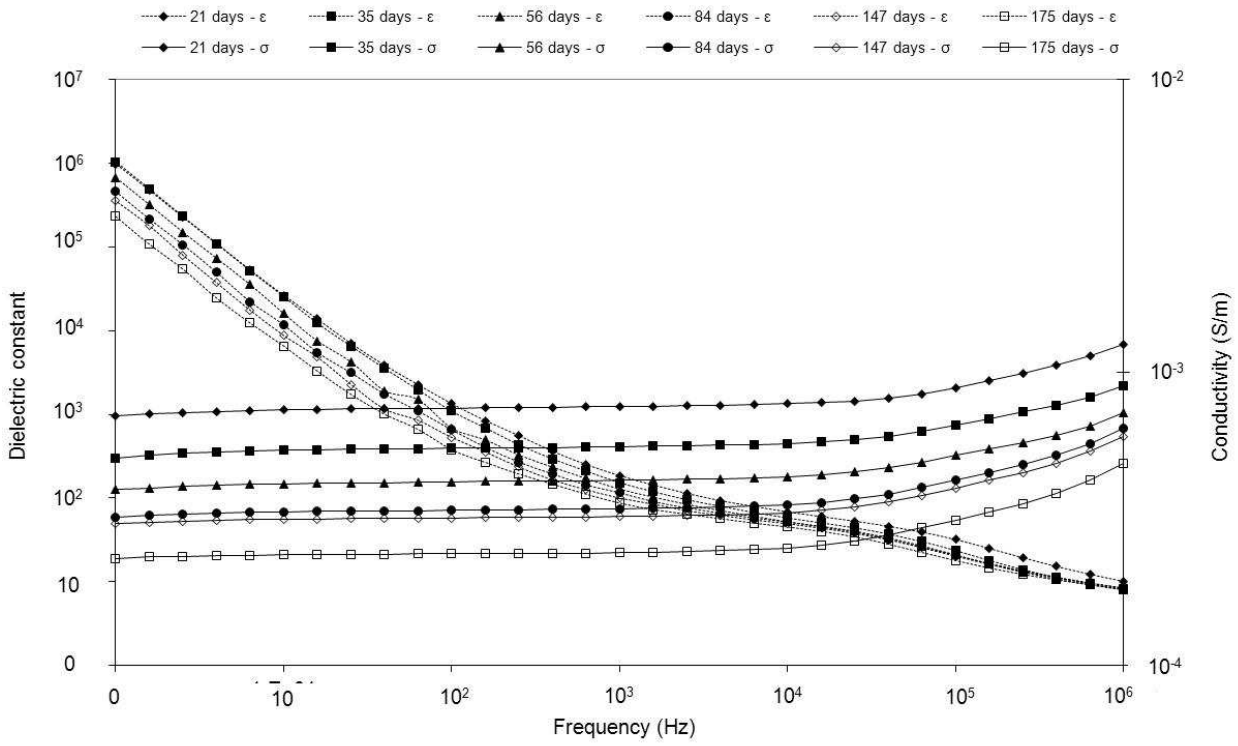

(a)

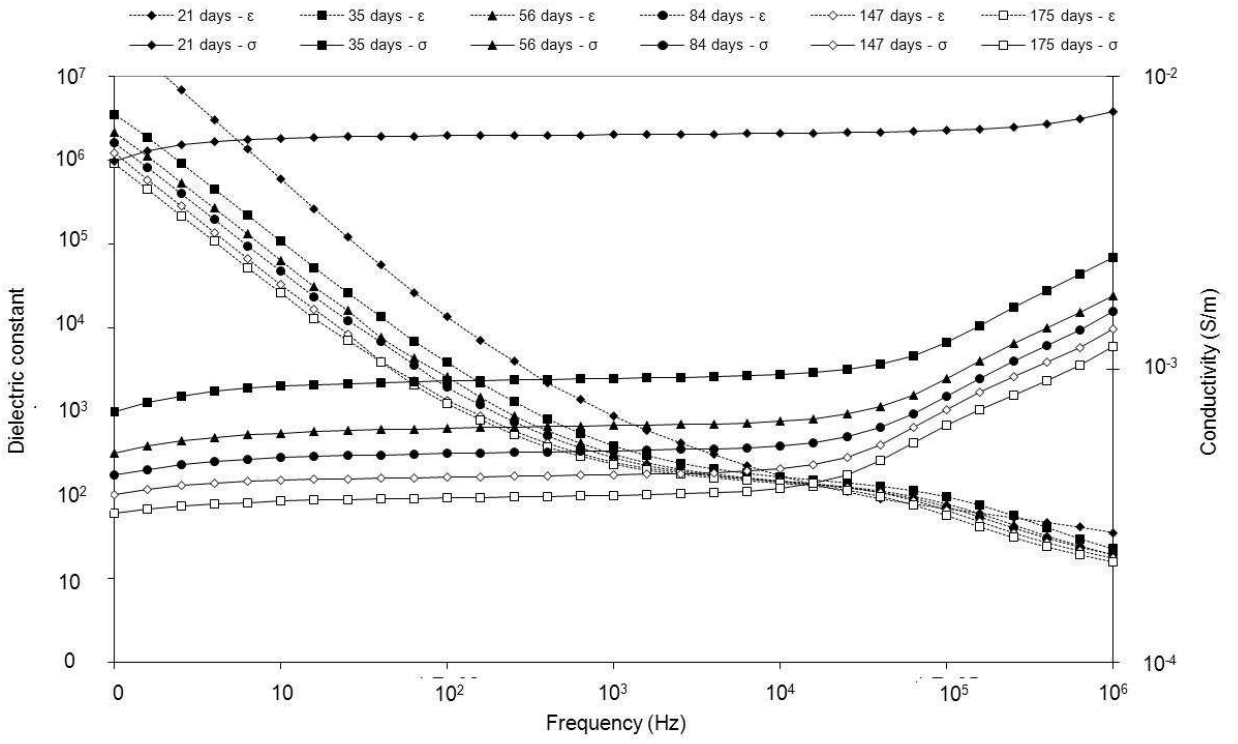

(b)

Figure 6: Typical plots of dielectric permittivity and conductivity for cuboidal samples of (a) NHL2, and (b) NHL5, between 21 and 175 days.

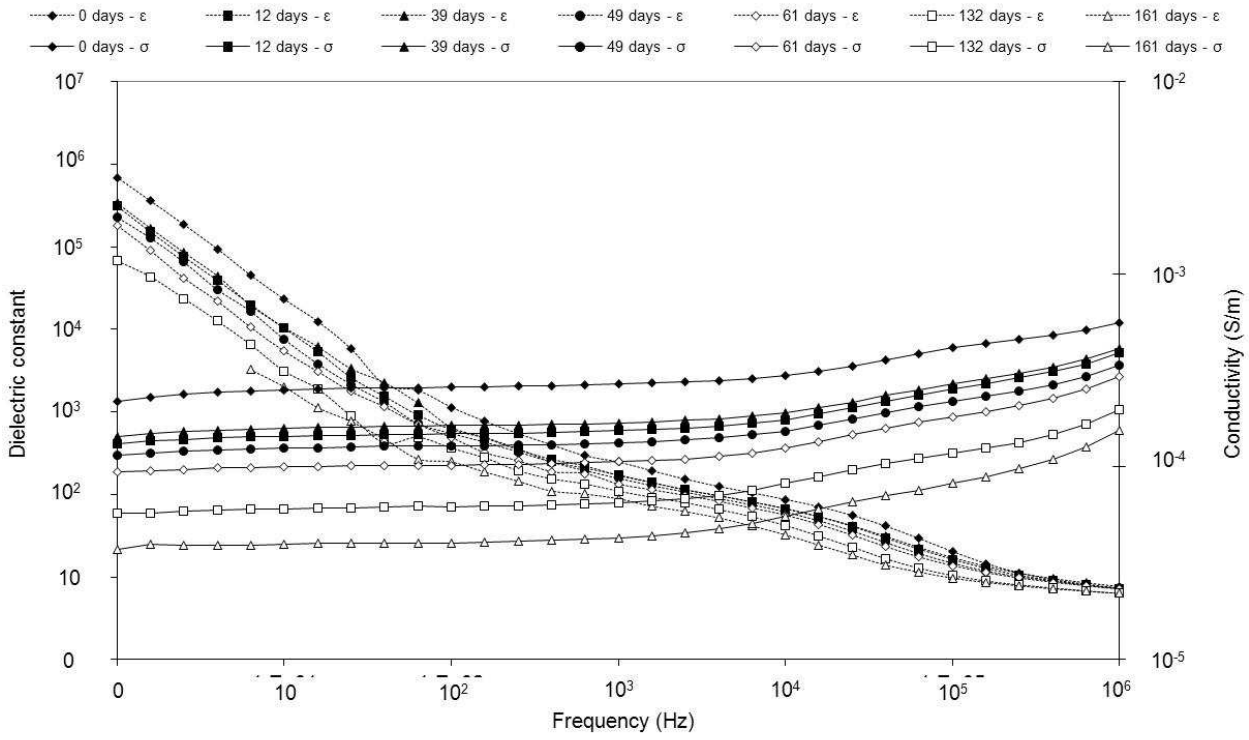

(a)

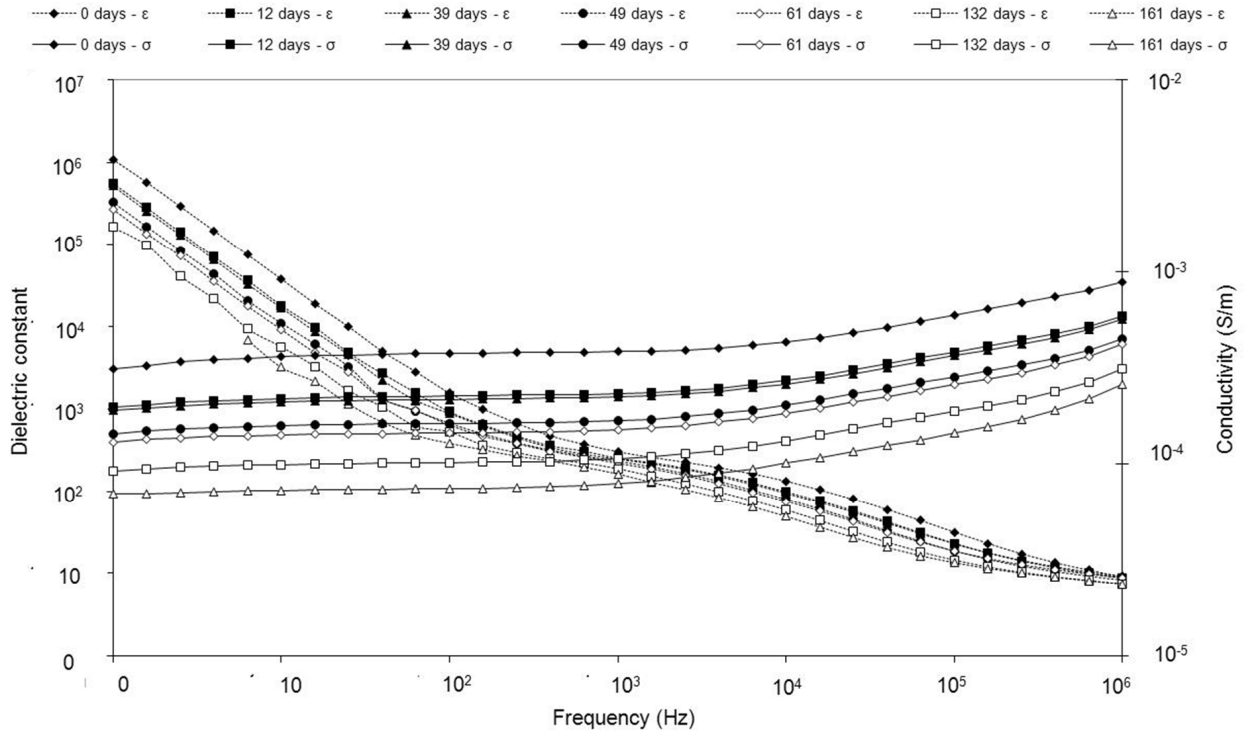

(b)

Figure 7: Typical plots of dielectric permittivity and conductivity for electrode pairs in NHL2 prismatic sample, (a) 5 mm location, and (b) 35 mm location, between 0 and 161 days.

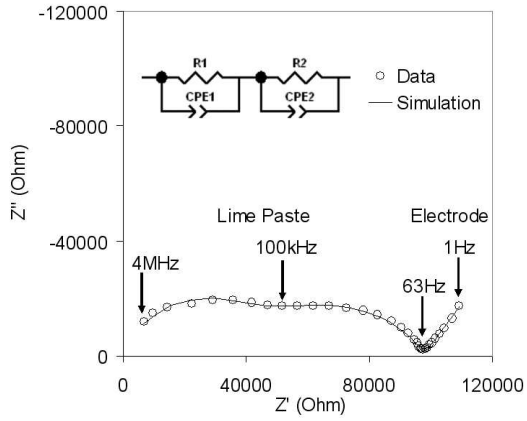

(a)

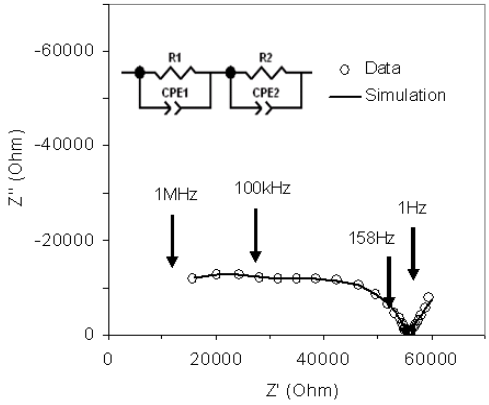

(b)

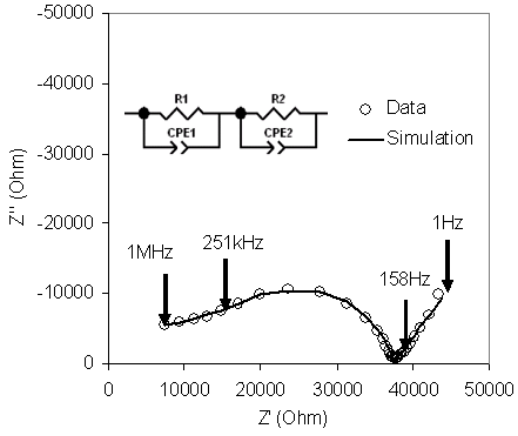

(c)

Figure 8: Typical complex plane plot and equivalent circuit parameters from simulation (a) prismatic NHL2 paste (at 5mm) after 12 days; (b) cuboidal NHL2 paste after 147 days and (c) cuboidal NHL5 paste after 147 days

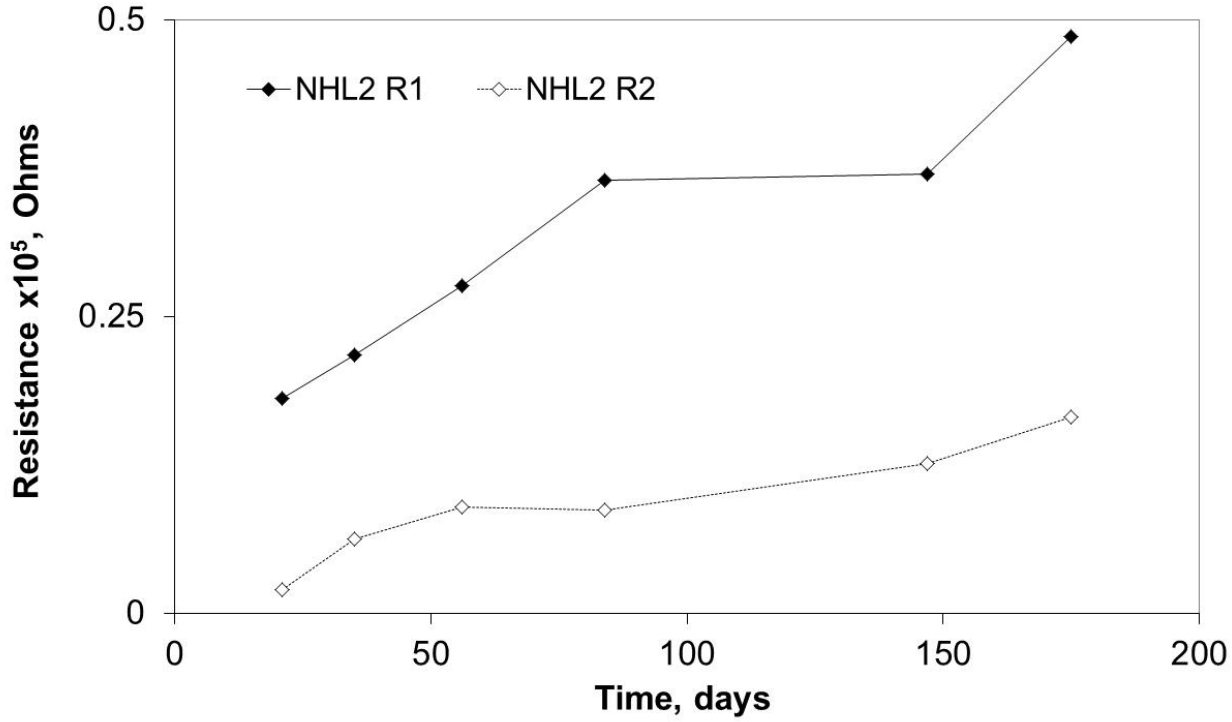

(a)

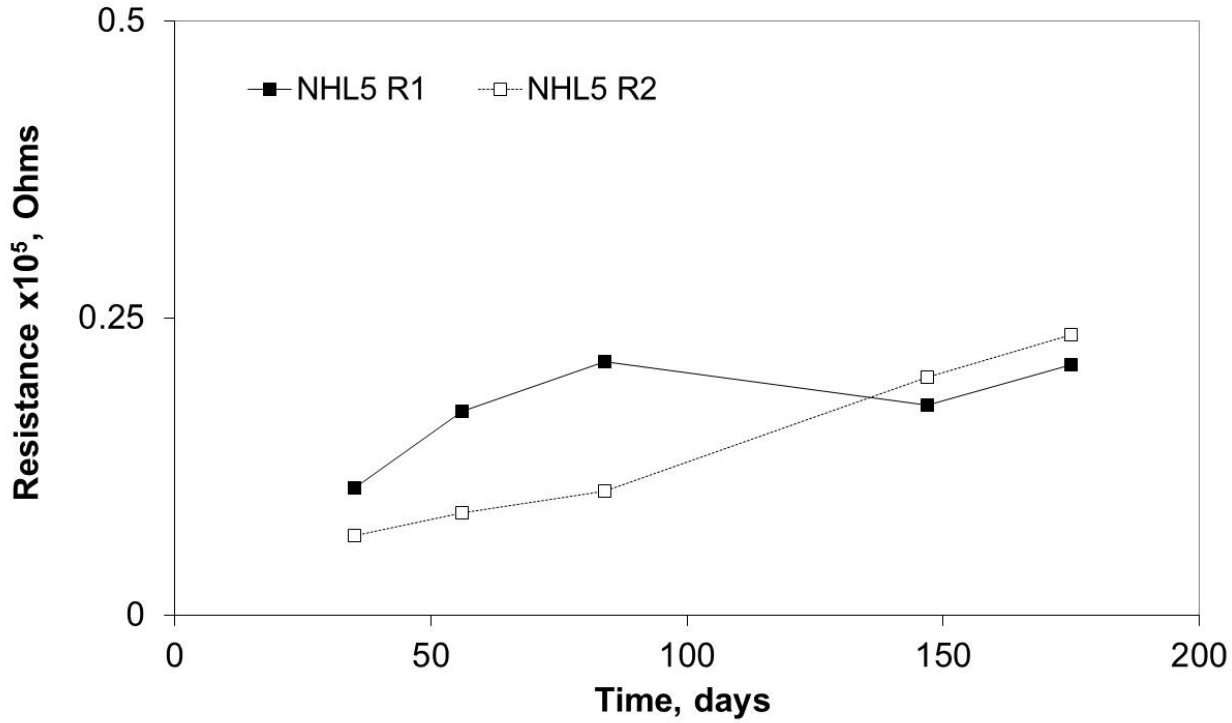

(b)

Figure 9: Values of R1 and R2 obtained from equivalent circuit modelling of complex plane plots obtained from (a) NHL2 and (b) NHL5 cuboidal samples.

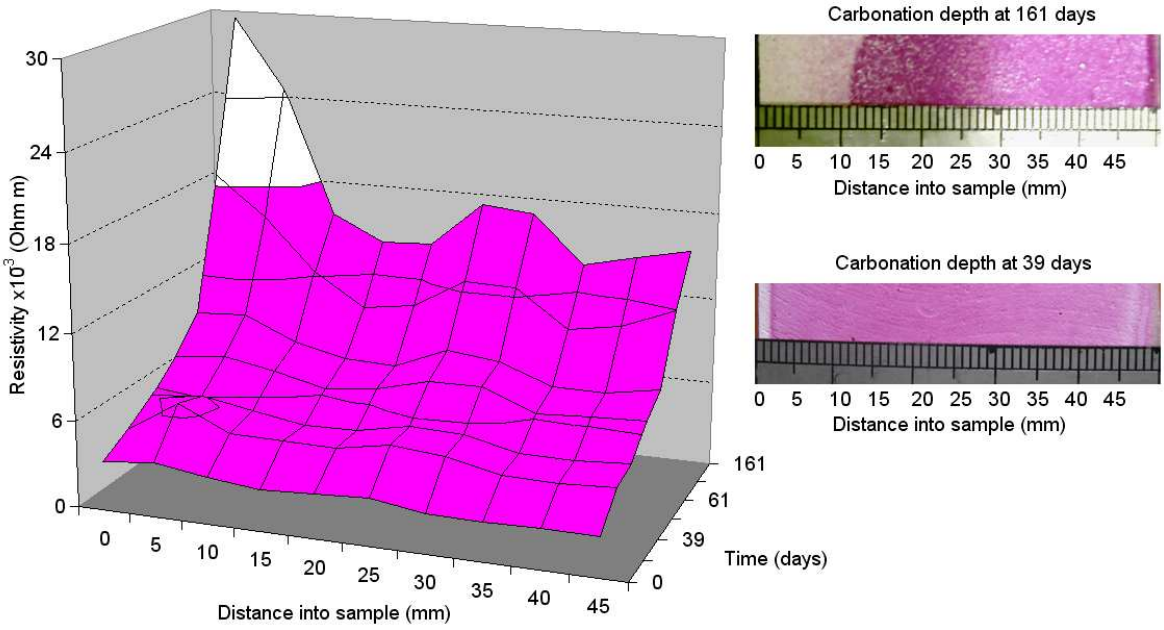

Figure 10: Contour plot showing resistivity of NHL2 lime paste between electrode pairs embedded in the prismatic samples. Images to the right show depth of carbonation revealed by phenolphthalein indicator.